Resonance Raman Excitation Profiles for the Permanganate Ion: Calculation of Franck–Condon Scattering Contributions for the Totally Symmetric Fundamental and Its Overtones and of the Equilibrium MnO Bond Length in the First $^1T_2$ Excited State

Robin J. H. Clark*,† and **Brian Stewart‡**

Contribution from the Christopher Ingold Laboratories, University College London, London WC1H OAJ, United Kingdom, and Department of Chemistry, University of Glasgow, Glasgow G12 8QQ, United Kingdom. Received February 20, 1981

Abstract: Detailed excitation profiles have been measured for the permanganate ion in the vicinity of the $^1T_2$ state at $\sim 19\,000$ cm^{-1}. Both [Ph$_4$P][MnO$_4$] and K[MnO$_4$]/K[ClO$_4$] mixed crystals have been studied, in each case using dye as well as ion laser excitation. The importance of interference terms in the Franck–Condon scattering mechanism is demonstrated. The analysis leads to an estimate for the change in equilibrium nuclear geometry resulting from the $^1T_2 \leftarrow {}^1A_1$ excitation. The change in the MnO equilibrium bond length, δ, was found to be 9.0 ± 0.5 pm for [Ph$_4$P][MnO$_4$] and 9.2 ± 0.5 pm for K[MnO$_4$]/K[ClO$_4$].

Studies on the excitation profiles of the $\nu_1(a_1)$ fundamental and its overtones of the [MnO$_4$]$^-$ ion were, until recently, restricted to data obtained with Ar$^+$ ion laser lines on the high energy side of the first $^1T_2 \leftarrow {}^1A_1$ (2e $\leftarrow$ t$_1$) transition of the ion in D$_2$O solution.[1] Mingardi et al.[2] have calculated the excitation profiles of these modes on the basis of a Franck–Condon scattering mechanism and by use of a shift parameter and damping factor appropriate to the relatively unresolved solution absorption spectrum of the ion. Although some agreement between experimental and calculated excitation profiles was obtained, the data then available and the analysis presented were insufficient for proper evaluation of the parameters of interest. The availability of Kr$^+$ ion laser lines and, in particular, dye laser lines prompted us to carry out a very thorough and detailed study of the excitation profiles of the ν_1, $2\nu_1$, and $3\nu_1$ bands of the [MnO$_4$]$^-$ ion in two solid-state environments. The first of these was K[MnO$_4$] isomorphously substituted into K[ClO$_4$], and some details of these results have already been reported.[3] The second form studied was the tetraphenylphosphonium salt, [Ph$_4$P][MnO$_4$]. In both cases, the $^1T_2 \leftarrow {}^1A_1$ band at $\sim 19\,000$ cm^{-1} shows clearly resolved vibronic structure, even at room temperature, and the excitation profiles of the ν_1, $2\nu_1$, and $3\nu_1$ bands proved to be very well resolved. Proper analysis of these results has allowed us to calculate with reasonable accuracy the change in the MnO equilibrium bond length resulting from the $^1T_2 \leftarrow {}^1A_1$ transition.

Experimental Section

The tetraphenylphosphonium salt of [MnO$_4$]$^-$ was prepared by the metathetical reaction between [Ph$_4$P]Br and K[MnO$_4$] in the minimum volume of water. The precipitated salt was filtered off and dried in vacuo. Tetraphenylphosphonium permanganate was mixed with K$_2$[SO$_4$] (as an internal standard) and pressed into disks which were spun during excitation to minimize heating effects.[4] For the same reason the laser power was kept below 120 mW at the sample.

The mixed crystal was prepared by dissolving K[ClO$_4$] containing approximately 5% w/w K[MnO$_4$] in hot water and allowing the solution to cool in a crystallizing dish. The crystals were washed in a little distilled water and dried in a vacuum dessicator. The proportion of K[MnO$_4$] was measured by preparing a standard solution of the mixed crystal and comparing the K[MnO$_4$] absorption at 530 nm to the absorption of solutions containing known amounts of K[MnO$_4$]. The amount of K[MnO$_4$] in the mixed crystal was determined to be 0.30%. The intensities of the [MnO$_4$]$^-$ ion bands were measured relative to that of the ν_1 band of the [ClO$_4$]$^-$ ion. Pressed disks of the sample were spun, and the laser power kept below 200 mW for the reasons given above.

Raman spectra were recorded on a Spex 1401 spectrometer and excitation was by various lines of Coherent Radiation CR12 Ar$^+$ and CR500 K Kr$^+$ lasers and, between 537 and 583 nm at 2-nm intervals, by a Coherent Radiation Model 490 dye laser employing sodium fluoroscein dye. Corrections were applied for the instrumental response and (via the intensity of the ν_1 band of the [SO$_4$]$^{2-}$ ion) for laser power variations. All band intensities were corrected for dependence on the fourth power of the wavenumber of scattered radiation, and band wavenumbers were calibrated against the emission lines of neon.

Visible absorption spectra were recorded by using a Cary 14 spectrometer. The wavenumber of the 0–0 band in the mixed crystal is independent of the percentage permanganate content in the range 0–3% permanganate (relevant to the present study), although it is increased monotonically with higher permanganate concentrations up to a maximum shift of 430 cm^{-1} at 100% permanganate.[5] The shift is related to the energy of interaction of the charge distribution of the excited ion with the host lattice.

Theory

General Basis of the Analysis. The theory to be outlined is that appropriate to the description of resonance Raman scattering intensities of totally symmetric vibrational modes for excitation into an electric-dipole-allowed electronic transition. The quantum mechanical expression for the $\rho\sigma$th element of the transition polarizability or scattering tensor is given by eq (1), where E, F,

$$[\alpha_{\rho\sigma}]_{FG} = \sum_E \left[\left(\frac{\langle F|\mu_\rho|E\rangle\langle E|\mu_\sigma|G\rangle}{E_E - E_G - E_L + i\Gamma_E} \right) + \left(\frac{\langle F|\mu_\sigma|E\rangle\langle E|\mu_\rho|G\rangle}{E_E - E_F + E_L + i\Gamma_E} \right) \right] \tag{1}$$

and G represent the excited, final, and ground vibronic states (energies E_E, E_F, and E_G, respectively), E_L is the laser energy, and the integrals in the numerators are the ρth and σth components of the transition dipole moments associated with the transition $E \leftarrow G$, etc.[6] The vibronic states may be written, using the Born–Oppenheimer approximation, as products of electronic and

(1) Kiefer, W.; Bernstein, H. J. *Mol. Phys.* **1972**, *23*, 835.
(2) Mingardi, M.; Siebrand, W.; van Labeke, D.; Jacon, M. *Chem. Phys. Lett.* **1975**, *31*, 208.
(3) Clark, R. J. H.; Cobbold, D. G.; Stewart, B. *Chem. Phys. Lett.* **1980**, *69*, 488.
(4) Kiefer, W. "Advances in Infrared and Raman Spectroscopy", Clark, R. J. H., Hester, R. E., Eds.; Heyden, London, 1977; Vol. 3, p 1.
(5) Teltow, J. *Z. Phys. Chem., Abt. B* **1938**, *B40*, 397.
(6) Clark, R. J. H.; Stewart, B. *Struct. Bonding (Berlin)* **1979**, *36*, 1.

† Christopher Ingold Laboratories.
‡ Department of Chemistry, University of Glasgow.

vibrational states. Further, for an electric-dipole-allowed transition, the nuclear coordinate dependence of the electric-dipole-moment operator may be neglected (Condon approximation). This leads to the factorization of the matrix elements of the polarizability tensor into pure vibrational overlap integrals and matrix elements of the electric-dipole operator involving only electronic coordinates. Restricting ourselves to a single, possibly degenerate, transition between the crude Born–Oppenheimer (CBO) electronic states $|g\rangle$ and $|e\rangle$, the transition polarizability becomes

$$[\alpha_{\rho\sigma}]_{g_n g_0} =$$

$$\langle g|\mu_\rho|e\rangle\langle e|\mu_\sigma|g\rangle\sum_v\left[\left(\frac{\langle n|v\rangle\langle v|0\rangle}{\epsilon_v + i\Gamma_v}\right) + \left(\frac{\langle n|v\rangle\langle v|0\rangle}{\epsilon_v^+ + i\Gamma_v}\right)\right] \quad (2)$$

where

$$\epsilon_v = E_{e_v} - E_{g_0} - E_L$$

$$\epsilon_v^+ = E_{e_v} - E_{g_n} + E_L$$

and

$$E_{e_v} - E_{g_n} = E_{00} + vhc\bar{\nu}' - nhc\bar{\nu}''$$

using the harmonic approximation for both ground- and excited-state vibrational potentials. E_{00} [$= E_e - E_g + {}^1/_2hc(\bar{\nu}'-\bar{\nu}'')$] is the energy of the 0–0 transition (electronic origin). E_L ($= hc\bar{\nu}_L$) is the energy of the exciting radiation of wavenumber $\bar{\nu}_L$, and Γ_v is the so-called damping factor or natural half-bandwidth (half-width at half-height) of the vth vibrational level of the chosen CBO excited electronic state $|e\rangle$. Equation 2 refers to a Stokes vibrational Raman transition creating n quanta in a single totally symmetric mode of the ground state. Only transitions originating from the zeroth vibrational level are considered, the Boltzmann population of higher levels being negligible for the complexes studied.

For a sample containing randomly oriented scatterers, the radiant intensity per scatterer at 90° to the direction of irradiation, $I_{\pi/2}$, is related to the product of $\alpha_{\rho\sigma}$ with its complex conjugate by

$$I_{\pi/2} = \left(\frac{10^8\pi^2}{\epsilon_0^2}\right)\mathcal{J}_L(\bar{\nu}_L - n\bar{\nu}'')^4\sum_{\rho,\sigma}\alpha_{\rho\sigma}\alpha_{\rho\sigma}^* \quad (3)$$

where $I_{\pi/2}$, ϵ_0 (the permittivity of free space), $\mathcal{J}_L$ (the irradiance of the incident exciting radiation), $\bar{\nu}$, and α are in W sr⁻¹, F m⁻¹, W m⁻², cm⁻¹, and F m², respectively. Substituting from eq 2 into eq 3 and expanding the square modulus gives us eq 4, where $|A_v|^2 = [\langle n|v\rangle\langle v|0\rangle]^2$ and $A_vA_{v'} = \langle n|v\rangle\langle v|0\rangle\langle n|v'\rangle\langle v'|0\rangle$. n refers to ground-state and v to excited-state vibrational quantum numbers throughout.

The dominant intensity contributions, for resonant and near-resonant excitation, are expected to arise from the terms A and D, which contain only resonance energy denominators. These two terms exemplify different kinds of excitation frequency dependence. Term A represents a sum of symmetrical Lorentzian curves, each of which peaks at a vibronic transition energy, that is, a series of vibronic resonances determined by $\epsilon_v = 0$ for $v = 0, 1, 2$, etc. Term D, in contrast, will not necessarily maximize at the energies of the vibronic resonances because it depends upon the resonance energy factors for pairs of vibrational levels. For this reason term D (and also terms E, F, and G) will be called an interference term. The interference can be either constructive or destructive at some particular excitation wavenumber since the
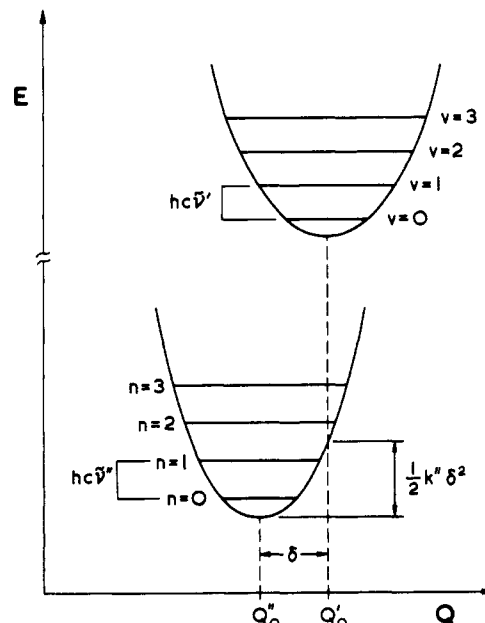

Figure 1. Schematic representation of the one-dimensional harmonic potential curves appropriate to the $\nu_1(a_1)$ mode of the [MnO₄]⁻ ion; $\bar{\nu}' = 0.9\ \bar{\nu}''$ and $k' = 0.8k''$.

D terms may be positive or negative. The net sign will depend first on the signs of the Franck–Condon factors $A_vA_{v'}$ (discussed in the next section) and second on the signs of the products of the resonance energy factors $\epsilon_v\epsilon_{v'}$. However, the relative importance of the latter depends on the magnitudes of the bandwidth products $\Gamma_v\Gamma_{v'}$.

Thus, because of the presence of the interference terms (predominantly term D), an excitation profile [the plot of Raman intensity against $\bar{\nu}_L$, which is normally corrected for $\mathcal{J}_L$ and $(\bar{\nu}_L - n\bar{\nu}'')^4$] will generally behave irregularly in the region of vibronic resonances. In particular, the peaks and troughs of the excitation profile need not follow those of the absorption profile. There are, however, two limiting cases in which the excitation profile and the absorption profile tend to conform with one another: (a) $\Gamma_v/hc\bar{\nu}' > {}^1/_2$ for all v, leading to smooth structureless absorption and excitation profile contours. In this case the excitation profiles for different overtones will generally maximize at different energies and none of these maxima need coincide with that of the absorption band contour. (b) $\Gamma_v/hc\bar{\nu}' \ll {}^1/_2$ for all v, leading to narrow, well-separated vibronic structure. The interference term D tends to insignificance relative to the term A in the limit as $(\Gamma_v/hc\bar{\nu}') \rightarrow 0$ since it is a function of ϵ_v^{-1} whereas the term A is a function of ϵ_v^{-2}. (The other interference terms are even smaller.) In this case the excitation profile maxima will coincide with the absorption profile maxima. However, the relative intensities in the two types of profile will differ due to the different Franck–Condon factors for the absorption and Raman processes.

Vibrational Overlap Integrals. The Franck–Condon overlap integrals between vibrational levels of the ground and excited states are calculated by using the model of one-dimensional harmonic potential-energy curves (Figure 1). If the ground- and excited-state fundamental wavenumbers, $\bar{\nu}''$ and $\bar{\nu}'$, respectively, are identical and so also are the respective equilibrium nuclear coordinates (Q_0'' and Q_0'), then the overlap matrix is a unit diagonal matrix. As a result absorption only occurs at the 0–0 position

$$I_{\pi/2} = \left(\frac{10^8\pi^2}{\epsilon_0^2}\right)\mathcal{J}_L(\bar{\nu}_L - n\bar{\nu}'')^4\sum_{\rho,\sigma}|\langle g|\mu_\rho|e\rangle\langle e|\mu_\sigma|g\rangle|^2\left[\underbrace{\sum_v|A_v|^2\left\{(\epsilon_v^2 + \Gamma_v^2)^{-1}}_{A} + \underbrace{\frac{2(\epsilon_v\epsilon_v^+ + \Gamma_v^2)}{(\epsilon_v^2 + \Gamma_v^2)[(\epsilon_v^+)^2 + \Gamma_v^2]}}_{B} + \underbrace{[(\epsilon_v^+)^2 + \Gamma_v^2]^{-1}\right\}}_{C}\right.$$

$$\left. + 2\sum_{v<v'}\sum A_vA_{v'}\left\{\underbrace{\frac{\epsilon_v\epsilon_{v'} + \Gamma_v\Gamma_{v'}}{(\epsilon_v^2 + \Gamma_v^2)(\epsilon_{v'}^2 + \Gamma_{v'}^2)}}_{D} + \underbrace{\frac{\epsilon_v\epsilon_{v'}^+ + \Gamma_v\Gamma_{v'}}{(\epsilon_v^2 + \Gamma_v^2)[(\epsilon_{v'}^+)^2 + \Gamma_{v'}^2]}}_{E} + \underbrace{\frac{\epsilon_v^+\epsilon_{v'} + \Gamma_v\Gamma_{v'}}{[(\epsilon_v^+)^2 + \Gamma_v^2](\epsilon_{v'}^2 + \Gamma_{v'}^2)}}_{F} + \underbrace{\frac{\epsilon_v^+\epsilon_{v'}^+ + \Gamma_v\Gamma_{v'}}{[(\epsilon_v^+)^2 + \Gamma_v^2][(\epsilon_{v'}^+)^2 + \Gamma_{v'}^2]}}_{G}\right\}\right] \quad (4)$$

and all Raman scattering is zero for the chosen vibrational mode. To obtain Raman scattering intensity it is sufficient that either $\bar{\nu}' \neq \bar{\nu}''$ or $\delta = Q_0' - Q_0'' \neq 0$. However, in real cases these two conditions are related since the redistribution of electrons resulting from an excitation both changes the force constants of a molecule and at the same time favors a different equilibrium nuclear geometry. The effect of the two conditions on the overlap matrix is quite different. In the first case, if $\delta = 0$ and $\bar{\nu}'' \neq \bar{\nu}'$, then nondiagonal overlaps $\langle v_e | n_g \rangle$ are nonzero provided $v - n$ is even, giving rise to only even harmonics (in particular, no fundamental) in the Raman spectrum through $\langle n|v \rangle \langle v|0 \rangle$, v even, n even. In the second case, when $\bar{\nu}' = \bar{\nu}''$ but $\delta \neq 0$, all nondiagonal overlaps become nonzero, and both even and odd harmonics appear in the Raman spectrum.

In this work the vibrational overlap integrals are computed via the recurrence relations of Manneback[7] from the $\langle 0|0 \rangle$ overlap which is given by the following expression:

$$\langle 0|0 \rangle = e^{(-1/2)\Delta^2}(k^+)^{1/2} \quad (5)$$

where

$$\Delta = \left(\frac{4\pi^2 c}{h}\right)^{1/2} \delta\mu^{1/2}\left(\frac{\bar{\nu}'\bar{\nu}''}{\bar{\nu}' + \bar{\nu}''}\right)^{1/2} \quad (6)$$

The dimensionless shift parameter, Δ, is conveniently written as

$$\Delta = 0.0017222 \delta\mu^{1/2}\left(\frac{\bar{\nu}'\bar{\nu}''}{\bar{\nu}' + \bar{\nu}''}\right)^{1/2} \quad (7)$$

for δ in pm, μ (the reduced mass) in u (amu), and $\bar{\nu}$ in cm^{-1}.[8] The recurrence relations are

$$\langle v + 1|n \rangle = -[v/(v + 1)]^{1/2}k\langle v - 1|n \rangle +$$
$$[n/(v + 1)]^{1/2}k^+\langle v|n - 1 \rangle - (v + 1)^{-1/2}a\langle v|n \rangle \quad (8)$$

and

$$\langle v|n + 1 \rangle = +[n/(n + 1)]^{1/2}k\langle v|n - 1 \rangle +$$
$$[v/(n + 1)]^{1/2}k^+\langle v - 1|n \rangle + (n + 1)^{-1/2}b\langle v|n \rangle \quad (9)$$

where

$$k = (\bar{\nu}'' - \bar{\nu}')/(\bar{\nu}'' + \bar{\nu}')$$

$$k^+ = 2(\bar{\nu}''\bar{\nu}')^{1/2}/(\bar{\nu}'' + \bar{\nu}')$$

$$a = \Delta[2\bar{\nu}''/(\bar{\nu}'' + \bar{\nu}')]^{1/2}$$

$$b = \Delta[2\bar{\nu}'/(\bar{\nu}'' + \bar{\nu}')]^{1/2}$$

The symmetries possessed by the Franck–Condon matrix under the four possible conditions of the parameters δ and $\bar{\nu}' - \bar{\nu}''$ are collected below.

$$\delta = 0, \bar{\nu}' = \bar{\nu}'': \text{ unit diagonal matrix}$$

$$\delta = 0, \bar{\nu}' \neq \bar{\nu}'': \langle v|n \rangle = (-1)^{(v-n)/2}\langle n|v \rangle, v - n \text{ even only}$$

$$\delta \neq 0, \bar{\nu}' = \bar{\nu}'': \langle v|n \rangle = (-1)^{v-n}\langle n|v \rangle$$

$$\delta \neq 0, \bar{\nu}' \neq \bar{\nu}'': |\langle v|n \rangle| \neq |\langle n|v \rangle|; \frac{\langle v|n \rangle}{|\langle v|n \rangle|} =$$
$$(-1)^{v-n}\left(\frac{\langle n|v \rangle}{|\langle n|v \rangle|}\right) \quad (10)$$

Calculations

The experimental data consist of relative Raman band intensities obtained by using an internal reference to correct for variation of incident irradiance $\mathcal{J}_L$. The data are also corrected for $\bar{\nu}_s^4$

(7) Manneback, C. *Physica* **1951**, *17*, 1001.
(8) The shift parameter, Δ, used here may be related to that of Mingardi and Siebrand, γ, if the approximation $\bar{\nu}' = \bar{\nu}''$ is adopted; in this circumstance, $\Delta^2 = k''\delta^2/2hc\bar{\nu}'' = \gamma$.

Table I. Parameters Used in Obtaining the Best-Fit Calculated Excitation Profiles

parameter	[Ph$_4$P]-[MnO$_4$]	K[MnO$_4$]/K[ClO$_4$]
$\bar{\nu}_{00}$, cm^{-1}	17 391	17 950
$\bar{\nu}_1''$, cm^{-1}	834	846
$\bar{\nu}_1'$, cm^{-1}	745	740
(Γ/hc), cm^{-1}	240	300
δ, pm	9.0	9.2
$\Gamma/hc\bar{\nu}'$	0.322	0.405
Δ^2	1.51	1.59

Table II. Franck–Condon Overlap Integrals, $\langle v|n \rangle$, Calcualted Using the Parameters Appropriate to [Ph$_4$P][MnO$_4$]^a

v	n				
	0	1	2	3	4
0	0.4691	0.5604	0.4921	0.3652	0.2421
1	-0.5929	-0.2399	0.1693	0.3894	0.4231
2	0.5112	-0.2265	-0.4105	-0.1555	0.1620
3	-0.3458	0.4710	0.1071	-0.3143	-0.3169
4	0.1936	-0.4592	0.2848	0.2988	-0.1214
5	-0.0920	0.3222	-0.4564	0.0672	0.3514
6	0.0375	-0.1801	0.4066	-0.3723	-0.1203
7	-0.0131	0.0834	-0.2666	0.4401	-0.2418
8	0.0039	-0.0324	0.1393	-0.3400	0.4251
9	-0.0009	0.0105	-0.0598	0.2002	-0.3925

^{a} See Table I. n refers to ground-state and v to excited-state vibrational quantum numbers.

Table III. Franck–Condon Overlap Integrals, $\langle v|n \rangle$, Calcualted Using the Parameters Appropriate to K[MnO$_4$]/K[ClO$_4$]^a

v	n				
	0	1	2	3	4
0	0.4522	0.5499	0.4943	0.3771	0.2579
1	-0.5880	-0.2640	0.1332	0.3638	0.4171
2	0.5193	-0.1981	-0.4092	-0.1897	0.1177
3	-0.3578	0.4623	0.1386	-0.2857	-0.3297
4	0.2026	-0.4676	0.2597	0.3166	-0.0776
5	-0.0964	0.3347	-0.4544	0.0337	0.3473
6	0.0388	-0.1885	0.4182	-0.3578	-0.1522
7	-0.0131	0.0866	-0.2780	0.4470	-0.2166
8	0.0036	-0.0327	0.1448	-0.3530	0.4244
9	-0.0007	0.0099	-0.0606	0.2083	-0.4051

^{a} See Table I. n refers to ground-state and v to excited-state vibrational quantum numbers.

dependence. Because of these facts, together with the assumption that the electronic transition is effectively isotropic, the calculations based on the terms in large square brackets of eq 4 are directly comparable with the observed excitation profiles. The assumption of isotropy means that any reduction in site symmetry from T_d is neglected. This appears to be justified since at the temperature of the experiments no splitting of the origin band is observed in the absorption spectrum.

As seen in the previous section, a complete overlap matrix can be calculated for a chosen set of values of the parameters μ, $\bar{\nu}'$, $\bar{\nu}''$, and δ. In practice, for a given vibrational mode, μ is fixed ($\mu = 16$ u for $\nu_1(a_1)$ of [MnO$_4$]$^-$) and $\bar{\nu}'$, $\bar{\nu}''$ are determined experimentally from the absorption and Raman spectra, respectively. Hence, a single variable parameter, δ, is needed to calculate the Franck–Condon matrix. A starting point for the calculations may be an estimate of δ obtained by fitting the relative oscillator strengths of the vibronic absorption bands.

$$f_{v0}/f_{00} = \bar{\nu}_{v0}[\langle v|0 \rangle]^2/\bar{\nu}_{00}[\langle 0|0 \rangle]^2$$

One of the advantages of the resonance Raman scattering method is, however, that δ is more accurately defined from excitation profiles than from absorption bands since the former refer to a single mode and are thus generally more resolved than an absorption spectrum, which is a convolution of bands often with
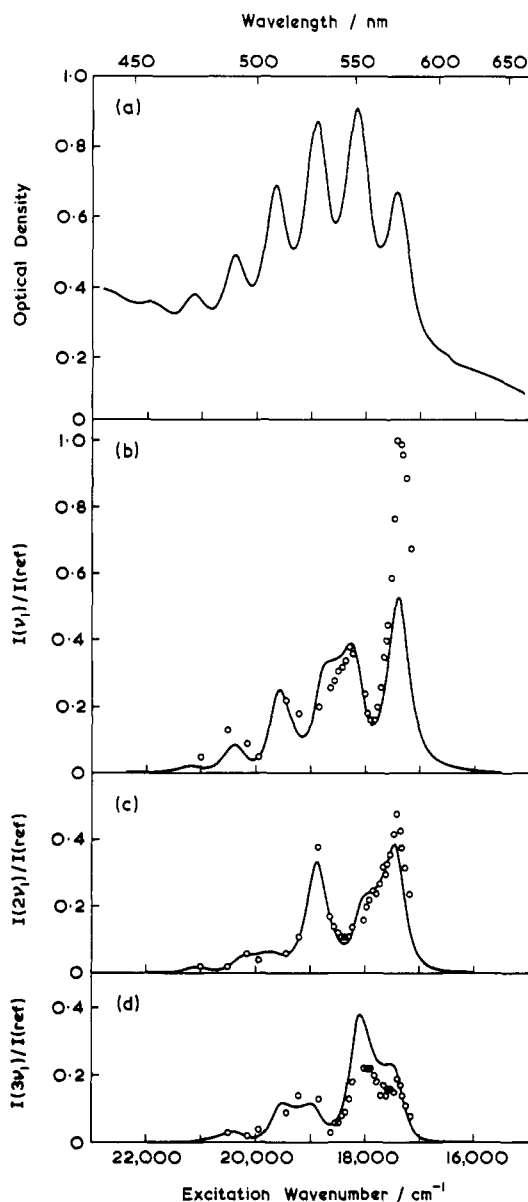
Figure 2. (a) Absorption spectrum of [Ph$_4$P][MnO$_4$] in an NaCl disk at room temperature in the region of the vibronically structured $^1T_2 \leftarrow$ $^1A_1$ band at $\sim$19000 cm^{-1}. (b)-(d) Experimental excitation profiles (O) for the ν_1, $2\nu_1$, and $3\nu_1$ bands, respectively, of [Ph$_4$P][MnO$_4$]. The full lines represent the (best-fit) calculated profiles for $\Gamma/hc = 240$ cm^{-1} and $\delta = 9.0$ pm.

Figure 3. (a) Absorption spectrum of K[MnO$_4$]/K[ClO$_4$] mixed crystal in a K[ClO$_4$] disk at room temperature. (b)-(d) Experimental excitation profiles (O) for ν_1, $2\nu_1$, and $3\nu_1$ bands, respectively, of K[MnO$_4$]/K[ClO$_4$] mixed crystal. The full lines represent the (best-fit) calculated profiles for $\Gamma/hc = 300$ cm^{-1} and $\delta = 9.2$ pm.

similar fundamental wavenumbers.

The Franck–Condon overlap matrix calculated by using the parameters appropriate to [Ph$_4$P][MnO$_4$] and K[MnO$_4$]/K[ClO$_4$] (see Table I) are shown in Tables II and III. For these values of the parameters δ and $\bar{\nu}'$, contributions to the scattering intensity from excited-state vibronic levels with $v > 9$ were negligible. The matrices show the asymmetry and sign structure consistent with the appropriate symmetry relations of eq 10. In order to display the relative importance of the wavenumber difference $(\bar{\nu}' - \bar{\nu}'')$ in the present case, the Franck–Condon matrix for [Ph$_4$P][MnO$_4$] calculated with $\delta = 0$ is shown in Table IV. Again this displays the expected symmetry. We may estimate the contribution to the scattering intensity of the first overtone brought about by the wavenumber difference from the overlap product $[\langle 2|v \rangle \langle v|0 \rangle]^2$ for $\delta = 0$. For example, for resonance with the 0–0 band, the contribution due to the wavenumber difference represents only about 3% of the total scattering intensity; i.e., $[\langle 2|0 \rangle \langle 0|0 \rangle]^2_{\delta=0,\bar{\nu}'\neq\bar{\nu}'}$ $\simeq 0.03[\langle 2|0 \rangle \langle 0|0 \rangle]^2_{\delta\neq0,\bar{\nu}'\neq\bar{\nu}'}$. This exemplifies the paramount importance of the shift parameter δ in determining the Franck–Condon scattering intensities.
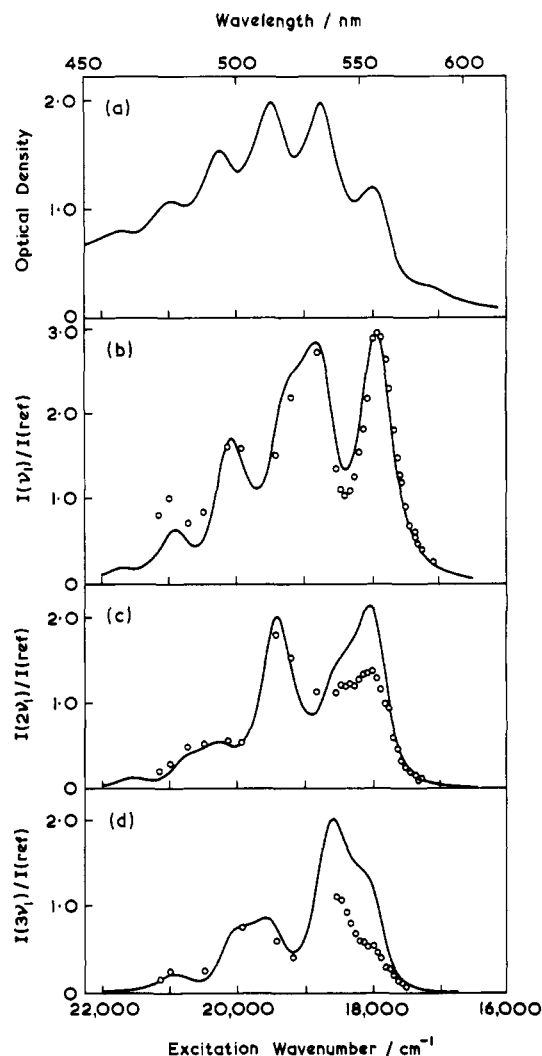
In order to calculate resonance Raman scattering intensity profiles (for a single mode) from the Franck–Condon overlap matrix, it is necessary to choose a set of bandwidth parameters, $\Gamma_{v'}$ and to identify the 0–0 band energy. In the present work it was found to be a very good approximation to assume that the bandwidths have a common value Γ, independent of v. In a relatively unresolved absorption spectrum the energy of the 0–0 band absorption maximum is not necessarily coincident with that of the true 0–0 transition. In an excitation profile the energy of the 0–0 resonance peak maximum is likely to be nearer the true 0–0 energy for reasons discussed above. There is still a deviation, however, due to the interference effects which are an important feature of vibronically structured excitation profiles. The excitation profile of the fundamental is the one which is least affected by interference effects in the region of the 0–0 resonance. These effects are illustrated later in Figure 6, in which it will be seen that there is a sign change in the interference terms in the region of the 0–0 energy. Since the negative contribution is on the low energy side, a blue shift of the 0–0 resonance peak maximum relative to the true 0–0 energy occurs. For the parameter values chosen for [Ph$_4$P][MnO$_4$] this shift in the ν_1 profile is 72 cm^{-1}.

The parameter values leading to the best fit between observed and calculated excitation profiles are given for [Ph$_4$P][MnO$_4$] in Table I, where they are compared with those for [MnO$_4$]$^-$ ion doped in K[ClO$_4$]. In order to compare calculated with observed relative Raman band intensities, the calculated profiles were scaled by a common normalization factor to produce agreement with

Table IV. Franck–Condon Overlap Integrals, $\langle v | n \rangle$, Calculated Using the Parameters[a] Appropriate to $[Ph_4P][MnO_4]$ but with $\delta = 0$

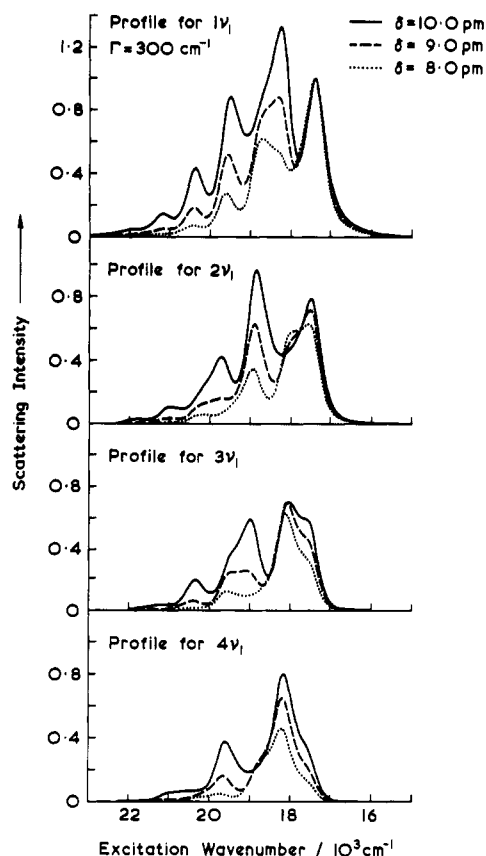| v	n				
	0	1	2	3	4
0	0.9992	0	0.0398	0	0.0019
1	0	0.9976	0	0.0689	0
2	−0.0398	0	0.9944	0	0.0972
3	0	−0.0689	0	0.9897	0
4	0.0019	0	−0.0972	0	0.9834
5	0	0.0043	0	−0.1250	0
6	−0.0001	0	0.0075	0	−0.1525
7	0	−0.0003	0	0.0114	0
8	5.274×10^{-6}	0	−0.0005	0	0.0161
9	0	1.58×10^{-5}	0	−0.0009	0

[a] See Table I.

Figure 4. Calculated excitation profiles for ν_1, $2\nu_1$, $3\nu_1$, and $4\nu_1$ of the $[MnO_4]^-$ ion with $\Gamma/hc = 300$ cm^{-1} and $\delta = 10.0$ pm (—), 9.0 pm (- - -), and 8.0 pm (···). The vibrational band wavenumbers are those observed for the $[Ph_4P]^+$ salt.

the observed profile of the fundamental at 18 250 cm^{-1}.

Results and Discussion

Change in Equilibrium Bond Length. The experimental absorption spectrum and excitation profiles for ν_1, $2\nu_1$, and $3\nu_1$ are shown in Figure 2 for $[Ph_4P][MnO_4]$ and in Figure 3 for K-$[MnO_4]$/K$[ClO_4]$, along with the (best-fit) excitation profiles calculated by using the parameter values given in Table I. Apart from an underestimate of the intensity of the 0–0 resonance peak for the fundamental in the $[Ph_4P]^+$ salt, the quality of the fit between calculated and experimental excitation profiles is excellent. However, it was impossible to produce a good fit to the complete $[Ph_4P][MnO_4]$ data (including the ν_1 0–0 resonance) by any combination of the parameters δ and Γ. Thus it was decided to leave the ν_1 0–0 resonance out of the fitting procedure. To give an impression of the significance of the fit, the effect on the calculated profiles of variations in δ and Γ are illustrated in Figures 4 and 5, respectively.

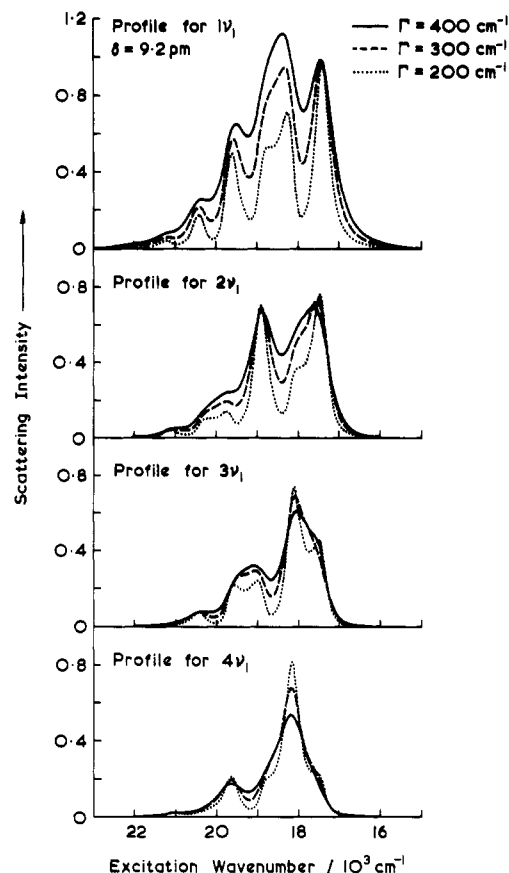**Figure 5.** Calculated excitation profiles for ν_1, $2\nu_1$, $3\nu_1$, and $4\nu_1$ of the $[MnO_4]^-$ ion with $\delta = 9.2$ pm and $\Gamma/hc = 400$ cm^{-1} (—), 300 cm^{-1} (- - -), and 200 cm^{-1} (···). The vibrational band wavenumbers are those observed for the $[Ph_4P]^+$ salt.

The value of Γ is effectively determined by the observed degree of resolution in the excitation profiles. As seen in Figure 5, the partially coalesced resonances (e.g., 0–1 and 0–2 for ν_1) are particularly sensitive in this respect. The value of Γ determined in this way is slightly smaller than the half-width at half-height of the 0–0 absorption band when the latter is measured from the low energy side. This is consistent with a small absorption intensity from hot-band transitions.

The calculated excitation profiles are sensitive to variations in δ as can be seen in Figure 4, where δ values of 8, 9, and 10 pm are used. In order to fit the relative intensities of the 0–0 and 0–1 resonance peaks for ν_1 (which we have chosen to regard as anomalous), a very much smaller value of δ (~ 7 pm) would be necessary, and this produces a worse fit in every other respect. In particular the relative intensities of the partially coalesced 0–1 and 0–2 resonances invert between 9 and 8 pm. This 0–1/0–2 region (18 000–19 000 cm^{-1}) is covered by dye laser excitation, and so one can be reasonably confident that the pattern of intensity variation is consistent with $\delta > 8$ pm and in fact with $\delta \sim 9$ pm. This is very similar to the δ value obtained for $[MnO_4]^-$ in K$[ClO_4]$ where no anomaly occurs in the ν_1 0–0 resonance region. Another δ-sensitive region covered by dye laser excitation is that of the 0–0/0–1 resonances for $2\nu_1$ (17 000–18 500 cm^{-1}). The observed pattern of intensity variation is again well reproduced by using $\delta = 9.0$ pm (see Figure 2). The agreement in this region would be significantly worse at lower δ values, as can be seen from Figure 4.

The relative intensities of the overtones are also sensitive to the value of δ. In general, higher overtones become relatively more intense with increasing δ. For example the 0–2 resonance peak for $2\nu_1$ at $\sim 18\,900$ cm^{-1} (Figure 4) crosses over the ν_1 excitation profile as δ increases from 8.0 to 9.0 to 10.0 pm.

We believe the semiquantitative considerations described above allow δ to be determined from the excitation profiles with fair confidence to within 0.5 pm.

Table V. Breakdown of Scattering Intensity Arising from the a_1 Fundamental Showing the Major Contributions at Two Laser Frequencies

| | | total scattering, % | |
| | | (a) | (b) |
v	v'	$\tilde{\nu}_L = \tilde{\nu}_{00} + {}^3/_2\tilde{\nu}'$	$\tilde{\nu}_L = \tilde{\nu}_{00}$
		Term A	
0		6.7	89.9
1		15.2	4.9
2		6.7	0.6
3		3.0	0.7
4		0.4	0.1
		32.0	96.2
		Term D	
0	1	+18.4	+15.8
0	2	+7.8	−2.9
0	3	+7.7	−2.1
0	4	+2.9	−0.7
0	5	+0.7	−0.2
1	2	+4.2	−3.4
1	3	+7.9	−3.6
1	4	+3.1	−1.6
1	5	+0.8	−0.4
2	3	+8.1	+1.3
2	4	+2.7	+0.6
2	5	+0.7	+0.2
3	4	+2.1	+0.6
3	5	+0.5	+0.2
4	5	+0.2	+0.1
		+67.8	+3.9
Terms (B + C) + (E + F + G)		+0.2	−0.1

^{a} All entries are expressed as the percentage of the total scattering at (a) $\tilde{\nu}_L = \tilde{\nu}_{00} + {}^3/_2\tilde{\nu}'$ and (b) $\tilde{\nu}_L = \tilde{\nu}_{00}$.

Interference Effects. A major qualitative feature of the excitation profiles is the coalescence of certain neighboring vibronic resonances. This phenomenon of the buildup of scattering intensity for excitation between levels results from the constructive interference effects involving pairs of vibronic levels, that is, positive contributions from terms D–G in eq 4. The positions of these constructive interferences correlate with the occurrence of nodes in the relevant Franck–Condon overlap products. By reference to Table II, it can be seen, for instance, that for the fundamental $\langle 1|v\rangle\langle v|0\rangle$ changes sign between $v = 1$ and $v = 2$ corresponding with the position of the large constructive interference observed in the ν_1 excitation profile. Similarly $\langle 2|v\rangle\langle v|0\rangle$ has nodes between $v = 0$ and $v = 1$ and between $v = 3$ and $v = 4$.

The position of the nodes, and hence of the constructive interferences, is dependent on the value of the shift parameter Δ. The extent of the effects is also modified by the magnitude of $\Gamma/hc\tilde{\nu}'$ and this is discussed further below. As can be seen in Table II, the node in $\langle 1|v\rangle\langle v|0\rangle$ occurs in the region of the Franck–Condon maximum for the absorption progression (maximum in $|\langle v|0\rangle|^2$), and this is generally the case.

Despite the above correlations, the pair of levels between which a constructive interference occurs does not itself provide the dominant contribution to the intensity buildup in the present cases. This is due to the effect of the magnitude of the bandwidths (Γ_v) relative to the vibronic level spacing $(hc\tilde{\nu}')$ in determining the magnitude of an interference contribution. Consider first the form that term D (the dominant interference term) of eq 4 takes in the ideal limit $\Gamma_v = 0$, $2\sum_v\sum_{v'}A_vA_{v'}/\epsilon_v\epsilon_{v'}$. Then for the fundamental scattering with excitation between levels 1 and 2 $(\tilde{\nu}_L = \tilde{\nu}_{00} + {}^3/_2\tilde{\nu}')$, the contribution from $v = 1$, $v' = 2$ is constructive since A_1A_2 is negative and so also is $\epsilon_1\epsilon_2$ $[= -{}^1/_4(hc\tilde{\nu}')^2]$. Similarly for all pairs of levels v, v' the contributions are positive. Now consider the effect of Γ becoming finite. The numerator of term D will become zero for the v, $v' = 1$, 2 contribution when $\Gamma^2 = -\epsilon_1\epsilon_2 = {}^1/_4(hc\tilde{\nu}')^2$
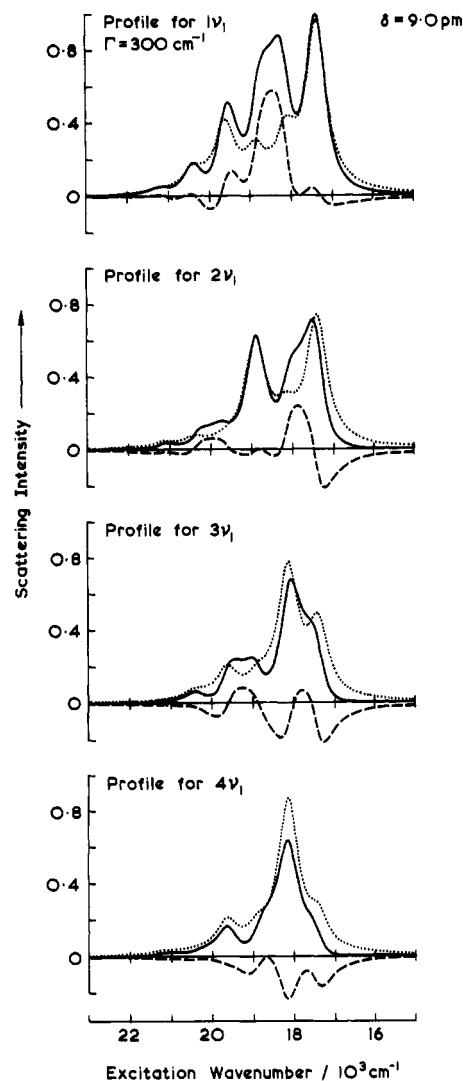

Figure 6. Calculated excitation profiles for ν_1, $2\nu_1$, $3\nu_1$, and $4\nu_1$ of $[Ph_4P][MnO_4]$ for $\Gamma/hc = 300$ cm^{-1} and $\delta = 9.0$ pm. The diagram illustrates the contributions from term A (···) and terms (B + C + D + E + F + G) (---) (in practice, predominantly term D) of eq 4 to the total scattering intensity (—).

or $\Gamma/hc\tilde{\nu}' = {}^1/_2$. In the case of the $[Ph_4P][MnO_4]$ calculation, $\Gamma/hc\tilde{\nu}' = 0.322$. For $[MnO_4]^-$ in $K[ClO_4]$, where $\Gamma/hc\tilde{\nu}' = 0.405$, a breakdown of the intensity contributions to the scattering by the fundamental is given in Table V, for (a) the constructive interference maximum $\tilde{\nu}_L = \tilde{\nu}_{00} + {}^3/_2\tilde{\nu}'$ and (b) the 0–0 resonance $\tilde{\nu}_L = \tilde{\nu}_{00}$. The excitation wavenumber dependence of the interference effects is illustrated in Figure 6, where term A (of eq 4) and the sum of terms B–G are plotted separately vs. $\tilde{\nu}_L$. From Table Va it can be seen that term D represents the major contribution to the scattering at $\tilde{\nu}_L = \tilde{\nu}_{00} + {}^3/_2\tilde{\nu}'$ and, since $\Gamma/hc\tilde{\nu}'$ < 0.5, all the D term contributions are still constructive. However, since the value of $\Gamma/hc\tilde{\nu}'$ is not very different from 0.5, the contribution from the v, $v' = 1$, 2 level pair in particular is only 4.2% of the total scattering. The major interference contribution arises in fact from the strongly scattering level pair v, $v' = 0$, 1 (18.4%). The situation is entirely different in the case of the exact resonance $\tilde{\nu}_L = \tilde{\nu}_{00}$ $(\epsilon_0 = 0)$ (Table Vb). Here the terms other than A are largely self-cancelling and the A term itself is dominated by the $\epsilon_0 = 0$ resonance which provides 89.9% of the total scattering. This is the typical result for any of the exact resonances $\epsilon_v = 0$ and is a demonstration of the truth of the maxim: the ordering of the intensities of the harmonics $n\nu_1$ at these exact resonances is correctly predicted by the relative magnitudes of the appropriate Franck–Condon factors $|\langle n|v\rangle\langle v|0\rangle|^2$. It must be noted that this is no longer necessarily true when $\Gamma/hc\tilde{\nu} > 0.5$, and so for structureless absorption bands there is no particular relation

between the order of overtone intensities and the Franck–Condon factors.

Conclusion

The present study of the [MnO$_4$]$^-$ ion illustrates the potential of resonance Raman band excitation profiles in determining the nature and magnitude of geometric changes in simple species consequent on excitation from the ground to the relevant excited state. These changes are more accurately defined in this way than they are from the absorption spectrum since the excitation profiles relate to a single mode and are thus better resolved than an absorption spectrum, which consists of a convolution of bands

arising from a variety of vibrational modes. The change so deduced in the equilibrium MnO bond length for the [MnO$_4$]$^-$ ion on ^{1}T$_2$ ← ^{1}A$_1$ excitation (~9.1 pm) is nevertheless similar to that estimated from the intensity distribution of the vibronic components of the ^{1}T$_2$ ← ^{1}A$_1$ absorption band (~10 pm).[9]

(9) Ballhausen, C. J. *Theoret. Chim. Acta* **1963**, *1*, 285.

Gas-Phase Generation of Phenylnitrene Anion Radical—Proton Affinity and $\Delta H_f°$ of PhN$^-$· and Its Clustering with ROH Molecules[1]

Richard N. McDonald,* A. Kasem Chowdhury, and D. W. Setser

Contribution from the Department of Chemistry, Kansas State University, Manhattan, Kansas 66506. Received April 10, 1981

Abstract: Phenylnitrene anion radical (PhN$^-$·) was prepared in a flowing afterglow apparatus by dissociative electron attachment to phenyl azide (PhN$_3$). PhN$^-$· undergoes a very slow reaction with PhN$_3$, producing PhN$_4$Ph$^-$· and PhN$_2$Ph$^-$· in a ratio of 4:1. The proton affinity of PhN$^-$· was bracketed from kinetic studies with various potential proton donors, PA(PhN$^-$·) = 372 ± 2 kcal mol^{-1}, from which $\Delta H_f°$(PhN$^-$·) = 60 ± 2 kcal mol^{-1} was calculated. With alcohols which are too weakly acidic to directly protonate PhN$^-$· [CH$_3$OH, C$_2$H$_5$OH, n-C$_3$H$_7$OH, and (CH$_3$)$_3$COH], a sequence of bimolecular reactions is observed involving ROH; PhN$^-$· → PhN$^-$·(HOR) → PhNH· + RO$^-$(HOR) → RO$^-$(HOR)$_x$. Although the first step of the sequence is slow, the second step, a cluster-to-cluster transformation, is fast. The related reaction sequence of PhN$^-$· reacting with HOH involves the ions PhN$^-$· → PhN$^-$·(HOH) → PhN$^-$·(HOH)$_2$ → PhNH· + HO$^-$(HOH)$_2$ → HO$^-$(HOH)$_x$ with the third reaction as the fast step. The relationship of these sequential processes to acidities and basicities found in solution is discussed. Of the five observed reaction channels for PhN$^-$· with CH$_3$CN, the major channel yields the adduct *m/z* 132 and a minor channel produces the M – 1 species, *m/z* 131. Additions by PhN$^-$· to C$_\alpha$ or N or CH$_3$CN are considered to account for these product anions. The reaction of PhN$^-$· with (CH$_3$)$_3$CCN also yields its adduct.

In the physical-organic chemistry of heteroatom-centered hypovalent ion radicals, the group 5a elements (N, P, As) are of interest since variations of the single attached alkyl or aryl groups permit studies of changes in the physical and chemical properties of these ion radicals. The simplest member of the series of nitrogen-centered hypovalent anion radicals, HN$^-$·, has been generated in the gas phase and thermodynamically characterized.[2] Our previous success in cleanly generating a carbene anion radical, c-C$_5$H$_4^-$·, by dissociative electron attachment to the corresponding diazo compound, c-C$_5$H$_4$N$_2$,[3] led us to consider the isoelectronic organic azides as precursors to nitrene anion radicals. To reduce the potential for N$_3^-$ ion formation, as observed from electron attachment to HN$_3$,[2] an aryl azide with a stronger C–N$_\alpha$ bond appeared to be desirable. The chemical[4] and electrochemical[5] reductions of phenyl azide (PhN$_3$) gave products consistent with formation of phenylnitrene anion radical (PhN$^-$·) as the first-formed intermediate. In the present work, we have successfully used the gas-phase electron attachment of PhN$_3$ to generate PhN$^-$· in a flowing afterglow apparatus and study the room temperature reactions of PhN$^-$· with PhN$_3$ and potential proton donors. In

later papers, we will report the results of studies of addition reactions of PhN$^-$· with various unsaturated molecules.[1]

Experimental Section

The flowing afterglow used in the investigation has been previously described.[3] Briefly, gas-phase anions are prepared by dissociative electron attachment to neutral reagents added to the helium buffer gas in the upstream end of flow tube. The carrier gas pressure (P_{He}) and flow velocity ($\bar{v}$) were maintained in the stainless steel flow tube (120 × 7.15 cm i.d.) by a Stokes Roots blower-mechanical pump system (Model 1722-S). However, these two parameters could be varied from P_{He} = 0.2–1.2 torr and $\bar{v}$ = 36–80 m/s by throttling a gate valve and/or altering the helium inlet flow. Our standard operating conditions were P_{He} = 0.5 torr and $\bar{v}$ = 80 m/s at 298 K.

In the present experiments, PhN$_3$ (~10^{12} molecules cm^{-3}) was introduced into the helium buffer gas before the carrier gas flowed past the electron gun. The negative ion composition of the flow monitored with an Extranuclear quadrupole mass spectrometer was *m/z* 91 (~99%) and *m/z* 26 (~1%, CN$^-$). When SF$_6$ was added to this flow via a port located 10 cm downstream of the electron gun, *no SF$_6^-$ signal was observed*, indicating high efficiency for electron attachment by the PhN$_3$ molecules; furthermore, destruction of the He*(2^{3}s) atoms generated by the electron gun also must be efficient.

The *m/z* 91 anions were thermalized by numerous collisions with the buffer gas as they flowed downstream (30 cm). At this point neutral reactant gases, Q, were added through a fixed inlet 61 cm from the first sampling nose cone; this is the ion–molecule reaction distance (time). Since this distance (time) is held constant during the experiment, variable concentrations of Q are added and the *m/z* 91 and product ion signals are recorded at each concentration of Q added to the flow. The slope from the log [PhN$^-$·] vs. Q concentration plot is then converted into the

(1) Paper 10 in the series "Hypovalent Radicals". For paper 9, see: McDonald, R. N.; Chowdhury, A. K. *J. Am. Chem. Soc.* **1981**, *103*, 674.

(2) Engelking, P. C.; Lineberger, W. C. *J. Chem. Phys.* **1976**, *65*, 4323 and references therein.

(3) McDonald, R. N.; Chowdhury, A. K.; Setser, D. W. *J. Am. Chem. Soc.* **1980**, *102*, 6491.

(4) Kauffman, T.; Hage, S. M. *Angew. Chem., Int. Ed. Engl.* **1963**, *2*, 156.

(5) McDonald, R. N.; Herbranson, D.; Hawley, M. D., unpublished results.